Chapter 6

Visualization of Single Dynein Molecules in Mammalian Cells

Nireekshit Addanki Tirumala and Vaishnavi Ananthanarayanan

Abstract

In vitro single-molecule imaging experiments have provided insight into the stepping behavior, force production, and activation of several molecular motors. However, due to the difficulty in visualizing single molecules of motor proteins in vivo, the physiological function and regulation of motors at the single-molecule level have not been studied widely. Here, we describe how highly inclined and laminated optical sheet (HILO) microscopy can be adapted to visualize single molecules of the motor protein cytoplasmic dynein-1 in mammalian cells with high signal-to-noise ratio and temporal resolution.

Key words Dynein, Single-molecule imaging, Live-cell imaging, Motor proteins

1 Introduction

Several studies on the behavior of cytoplasmic dynein-1 ("dynein" hereafter) have relied on visualizing the dynamics of dynein along microtubules conjugated to the coverslip [1–6]. The evanescent field created in total internal reflection fluorescence (TIRF) microscopy [7] allows for imaging only those molecules that are bound to the microtubules. By using low concentrations of fluorescent motors, only a few molecules are bound to the microtubules at a given time, and therefore, individual dynein molecules can be visualized and tracked. Thus, in vitro single-molecule studies have provided significant insight into the stepping behavior [1], activation [3, 5, 8], and force production by dynein [9, 10]. Extending these observations and findings to living cells is essential to advance our understanding of dynein.

However, visualizing single molecules of dynein in live mammalian cells poses several challenges:

1. Inside the cell, microtubules are up to ~1 μm away from the coverslip, separated by the plasma membrane and cortical actin.

Steven M. Markus (ed.), *Dynein: Methods and Protocols*,
Methods in Molecular Biology, vol. 2623, https://doi.org/10.1007/978-1-0716-2958-1_6,

This rules out using conventional TIRF microscopy for imaging dynein interacting with microtubules and cargo in living cells.

2. Epifluorescence fluorescence microscopy suffers from poor signal-to-noise ratio owing to fluorescence from multiple planes, thereby making it difficult to distinguish single molecules.
3. Point scanning confocal microscopy that can overcome the limitation of signal from multiple planes suffers from poor temporal resolution thereby making it hard to track the fast single-molecule dynamics.

Highly inclined and laminated optical sheet (HILO) microscopy [11] offers the optimal compromise between TIRF and epifluorescence techniques. In HILO microscopy, the incident excitation laser is sent at an angle slightly less than the critical angle, thereby illuminating the sample obliquely with a narrow sheet of light, significantly increasing the signal-to-noise ratio (SNR). HILO microscopy has been previously used to visualize single molecules of dynein in *S. pombe* [12, 13] *and S. cerevisiae* [14]. In this chapter, we describe additional steps required to optimize HILO microscopy to visualize single molecules of dynein in living mammalian cells [15].

2 Materials

2.1 Cell Culture

1. Mammalian cells expressing fluorescently tagged dynein. In procedures described in this chapter, we use HeLa cells expressing mouse dynein heavy-chain 1 tagged with GFP (mDHC-GFP) [16].
2. Medium for HeLa cell culture: Dulbecco's modified Eagle's media (DMEM) containing 4.5 gm glucose/liter, 2 mM L-glutamine, 1000 units/mL penicillin, 1 mg/mL streptomycin, 400 μg/mL G418, 10% fetal bovine serum, and pH adjusted to 7.6.
3. Live-cell imaging solution: Sterile ultra-pure water with 4.5 gm glucose/liter, 140 mM NaCl, 2.5 mM KCl, 1.8 mM $CaCl_2$, 1.0 mM $MgCl_2$, 20 mM HEPES, and pH adjusted to 7.4.
4. Glass-bottom (coverslip no. 1.5) imaging dishes.

2.2 Microscopy

1. Laser source (488 nm, 100 mW at source).
2. TIRF module with field stop.
3. Inverted microscope body.
4. Filter cube with excitation filter (488/50 nm bandpass), longpass beam splitter (488 nm single edge), emission filter (520/28 nm bandpass).

5. 1.49 NA, 100× TIRF objective.
6. Microscope stage with stage top incubator.
7. Andor iXon Ultra 897 EMCCD camera (or similar suitable ultrasensitive camera).
8. Desktop computer with software to control the microscope and store data.

3 Methods

3.1 Sample Preparation

1. 48 h prior to imaging, plate the cells in glass-bottom imaging dishes such that they are ~60% confluent at the time of imaging (*see* **Note 1**). To enhance adhesion of cells to the glass bottom, the dishes can be treated with poly-D-lysine for 60 min and washed well prior to seeding the cells.
2. Grow cells in complete media in an incubator maintained at 37 °C and 5% CO_2.
3. Prior to imaging, wash the cells gently with live-cell imaging solution warmed to 37 °C.

3.2 Microscopy

1. Place the sample on the microscope stage top incubator and bring the cells into focus.
2. Turn on the excitation laser at low power to avoid photobleaching the sample. Using the TIRF module, adjust the incident beam to the center of the objective rear aperture (*see* **Note 2**).
3. Adjust the TIRF module to focus the incident laser beam at the objective back focal plane. If done correctly, **Steps 2** and **3** should ensure that a very narrow collimated beam of light exits the objective (Fig. 1a).
4. Using the TIRF module moves the incident laser beam away from the center of the TIRF objective back focal plane. This should lead to the excitation beam exiting the objective obliquely (Fig. 1b).
5. Continue moving the incident laser beam until total internal reflection occurs. For oil ($n = 1.52$)–water ($n = 1.36$) interface, total internal reflection occurs when the incident angle is approximately 63° (Fig. 1c). The transition to TIR is marked by a sharp increase in signal-to-noise ratio when visualized through the camera.
6. Place a field stop in the light path at a position conjugate to the sample focal plane. Reduce the diameter of the field stop such that the width of the incident beam as observed on the camera is approximately 30 μm (Fig. 1c, *see* **Note 3**).

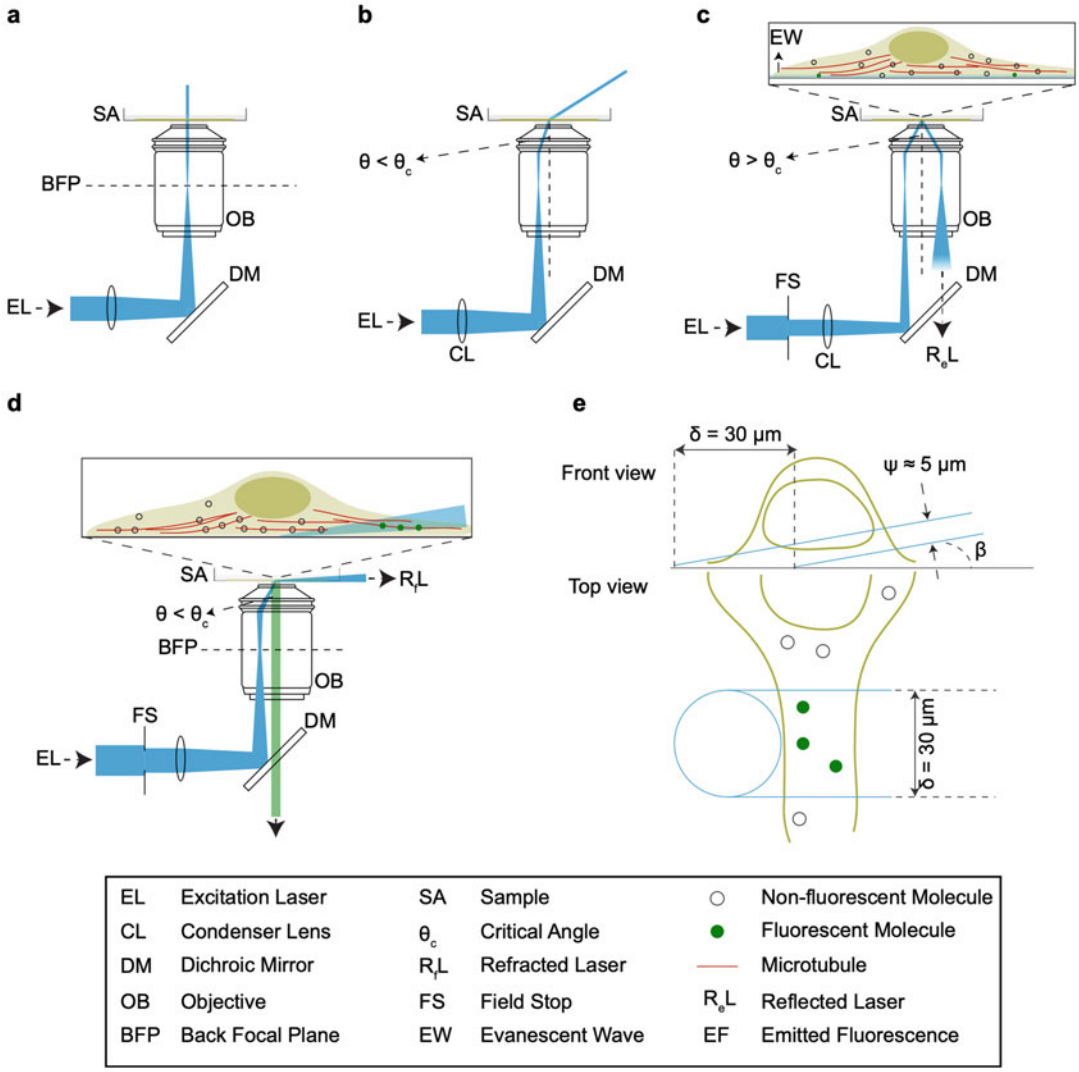

Fig. 1 Steps in setting up HILO microscopy to visualize single molecules of dynein in mammalian cells. (**a**) Excitation laser focused at the center of the objective back focal plane. (**b**) Excitation laser focused off center at the objective back focal plane leading to refraction at oil–water interface. (**c**) Field stop inserted into light path and excitation laser incident at an angle > critical angle ($\theta > \theta_c$) causing total internal reflection (TIR). (**d**) Excitation laser incident at an angle less than critical angle ($\theta < \theta_c$) leading to highly inclined and laminated optical sheet (HILO) illumination. (**e**) Illustration of a cell under HILO microscopy.

7. Use the TIRF module and reduce the incident laser angle to approximately 60° to exit the TIR state. This should lead to a thin sheet of light illuminating the sample plane (Fig. 1d).
8. Adjust the orientation of the incident beam (by using the TIRF module if possible) and the position of a cell (by moving the stage) such that the incident beam is perpendicular to the major axis of the cell (Fig. 1e, *see* **Note 4**).

9. Depending on the morphology of the cell, adjust the incident laser angle between 60° and 63° to a point where the cell is the brightest.
10. Acquiring continuous image stream at 50 frames per second should lead to visualization of fluorescent spots of dynein. On an Andor iXon 897 camera, the following settings were used to acquire images at 50 frames per second with no interval between frames.
    - Exposure—20 ms
    - Frame transfer—On
    - Vertical clock speed—0.3 μs
    - Vertical clock voltage—+4
11. To verify if the microscope settings are correct (*see* **Note 5**), create a kymograph from the time series acquired in the earlier step. Distinct fluorescent traces corresponding to either moving or stationary particles should be clearly visible (Fig. 2).
12. If not, repeat **step 9**. The optimum incident laser angle is dependent on the morphology of the particular cell being visualized.

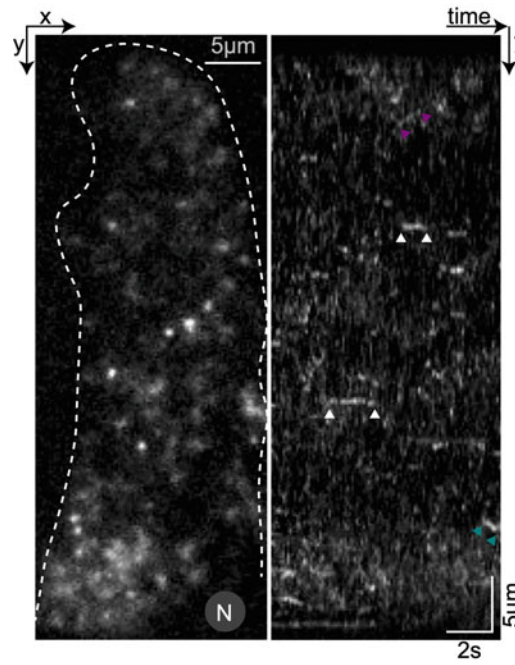

Fig. 2 Image analysis and verification of single-molecule imaging. Left, a single frame from a 10-s long, 10 fps video of a HeLa cell expressing mDHC-GFP, and imaged used HILO microscopy. Right, a kymograph showing fluorescent traces of dynein. White, teal, and magenta arrowheads represent stationary, minus-end moving, and plus-end moving molecules, respectively. "N" represents the location of the nucleus

3.3 Image Analysis and Verification

The time series obtained can then be used in combination with single-particle tracking software such as μTrack [17] or low light tracking tool [18]. Confirmation of single-molecule visualization can be performed in many ways including intensity histogram analysis and stepwise photobleaching [12, 15].

4 Notes

1. The cell confluence at the time of imaging influences the signal-to-noise ratio. Best results are obtained when there is only one cell within the field of view of imaging. This ensures that the incident laser beam excites fluorophores only in the cell of interest thus providing superior signal-to-noise ratio. However, this has to be balanced with the optimum confluence for a healthy culture of the specific cell line being used in the study. For the HeLa cells we used, 60% seeding density provided optimum conditions for single-molecule imaging 48 h later.
2. The following procedure can be used to check if the incident laser beam is centered.
   (a) Carefully bring a sheet of paper close to the objective such that the plane of the paper is normal to the objective axis. Mark a cross-hair at the point on the sheet which is right above the objective center.
   (b) If the incident laser is centered, then it will consistently fall on the cross-hair even when the sheet of paper is at different distances from the objective.
3. The diameter (δ in Fig. 1) of the incident beam should ideally be chosen such that only the region of the cell from which data are being collected is illuminated. Furthermore, the thickness (ψ in Fig. 1) of the beam is related to the incident beam diameter as $\psi = \delta^{*}\sin(\beta)$. Small values of ψ result in higher light density in the HILO sheet but is achieved by comprising on the illuminated region of interest. For example, Fig. 2 was obtained with the $\delta = 30$ μm, $\theta \approx 60°$ and therefore $\psi \approx 19$ μm.
4. An incident beam that is perpendicular to the cell ensures that the region of the cell being observed is illuminated by a beam of uniform thickness, thus guaranteeing consistent intensity values of fluorophores from the ROI.
5. The frame rate for image acquisition and analysis should be chosen in accordance with the cellular process of interest. For example, in kymographs obtained from 50 fps time series, a majority of the traces are faint, bidirectional, and random. These most likely represent dynein freely diffusing in the cytosol. Hence, high frame rate acquisition and subsequent tracking might be useful to quantify the cytosolic diffusion of single

dynein molecules. Reducing the frame rate to 10 fps by using a sliding average eliminates the diffusive traces from the kymograph and retains only traces corresponding to dynein bound to microtubules. Averaging significantly improves signal-to-noise ratio as well. Thus, analyzing at lower frame rates might help in visualizing traces of dynein binding to microtubules, moving and unbinding from it.

References

1. Reck-Peterson SL, Yildiz A, Carter AP et al (2006) Single-molecule analysis of dynein processivity and stepping behavior. Cell 126:335–348
2. Ross JL, Wallace K, Shuman H et al (2006) Processive bidirectional motion of dynein-dynactin complexes in vitro. Nat Cell Biol 8: 562–570
3. Trokter M, Muckec N, Surrey T (2012) Reconstitution of the human cytoplasmic dynein complex. Proc Natl Acad Sci U S A 109:20895–20900
4. Kardon JR, Reck-Peterson SL, Vale RD (2009) Regulation of the processivity and intracellular localization of Saccharomyces cerevisiae dynein by dynactin. Proc Natl Acad Sci 106:5669–5674
5. McKenney RJ, Huynh W, Tanenbaum ME et al (2014) Activation of cytoplasmic dynein motility by dynactin-cargo adapter complexes. Science 80-) 345:337–341
6. McKenney RJ, Huynh W, Vale RD, Sirajuddin M (2016) Tyrosination of α-tubulin controls the initiation of processive dynein–dynactin motility. EMBO J 35:1175–1185
7. Axelrod D (2015) Total internal reflection fluorescence microscopy. Encycl Cell Biol 2: 62–69
8. Schlager MA, Hoang HT, Urnavicius L et al (2014) In vitro reconstitution of a highly processive recombinant human dynein complex. EMBO J 33:1855–1868
9. Brenner S, Berger F, Rao L et al (2020) Force production of human cytoplasmic dynein is limited by its processivity. Sci Adv 6:1–12
10. Elshenawy MM, Kusakci E, Volz S et al (2020) Lis1 activates dynein motility by modulating its pairing with dynactin. Nat Cell Biol 22:570–578
11. Tokunaga M, Imamoto N, Sakata-Sogawa K (2008) Highly inclined thin illumination enables clear single-molecule imaging in cells. Nat Methods 5:159–161
12. Ananthanarayanan V, Schattat M, Vogel SK et al (2013) Dynein motion switches from diffusive to directed upon cortical anchoring. Cell 153:1526–1536
13. Ananthanarayanan V, Tolić IM (2015) Single-molecule imaging of cytoplasmic dynein in vivo. Methods Cell Biol 125:1–12
14. Lammers LG, Markus SM (2015) The dynein cortical anchor Num1 activates dynein motility by relieving Pac1/LIS1-mediated inhibition. J Cell Biol 211:309–322
15. Tirumala NA, Redpath G, Dolai P et al (2021) Single-molecule imaging of cytoplasmic dynein in cellulo reveals the mechanism of motor activation and cargo capture. bioRxiv 2021.04.05.438428
16. Poser I, Sarov M, Hutchins JRA et al (2008) BAC TransgeneOmics: a high-throughput method for exploration of protein function in mammals. Nat Methods 5:409–415
17. Jaqaman K, Loerke D, Mettlen M et al (2008) Robust single-particle tracking in live-cell time-lapse sequences. Nat Methods 5:695–702
18. Krull A, Steinborn A, Ananthanarayanan V et al (2014) A divide and conquer strategy for the maximum likelihood localization of low intensity objects. Opt Express 22:210